Time-resolved photoluminescence study of AgCl:Cd^{2+} crystalline foils: excitation energy transfer

1995 J. Phys.: Condens. Matter 7 433

(http://iopscience.iop.org/0953-8984/7/2/021)

J. Phys.: Condens. Matter 7 (1995) 433–446. Printed in the UK

Time-resolved photoluminescence study of AgCl:Cd^{2+} crystalline foils: excitation energy transfer

Jan Valenta, Ivan Pelant†, Věra Kohlová, Věra Bradnová‡, Miroslava Trchová, Josef Klimovič and Jan Hála

Charles University, Faculty of Mathematics and Physics, Ke Karlovu 3, 121 16 Prague 2, Czech Republic

Received 6 May 1994, in final form 15 September 1994

Abstract. Crystalline AgCl:Cd^{2+} thin foils (Cd^{2+} concentration 62.5–5000 ppm) were studied by time-resolved photoluminescence spectroscopy in the temperature range 20–80 K using a mechanical phosphoroscope. It has been found that the emission spectrum consists of two bands, located at ~ 480 nm ('blue') and ~ 590 nm ('red'). With increasing delay after excitation (3–100 ms), the emission spectrum shifts considerably to the red region. Similarly, a temperature increase at fixed delay results in a red-shifted spectrum. To explain these results, a simple kinetic model is suggested supporting the existence of two radiative channels: (i) self-trapped exciton and (ii) a nearby Cd^{2+} emission centre. A simple method is presented for how to use the photoluminescence behaviour to check the suitability of AgCl:Cd^{2+} foils to record high-energy-particle tracks.

1. Introduction

The extraordinary photochemical behaviour of silver halides has been known for a long time. Silver bromide and silver chloride are the most important components of photographic emulsions. Special types of AgCl photographic emulsions are frequently used as nuclear-track detectors. From the early 1970s doped silver chloride crystalline sheets (so-called solid-state nuclear-track detectors) have also been studied [1] with the aim of replacing emulsions in some special experiments (for example in satellites [2]). They display two main advantages. First, the development of a latent image in the sheets is a simple photophysical procedure (an exposure to blue-ultraviolet light) and consequently no mechanical distortions are produced during the development, in contrast to emulsions developed in liquid chemicals. Secondly, the latent images of tracks must be stabilized by exposing the sheets to nonactinic (e.g yellow) light during the period when particles are passing through. So one has a simple possibility to switch on/off the detection at a desired moment. The detectors are usually made of cadmium-doped silver chloride [3]. Some parameters of these AgCl:Cd^{2+} detectors, however, are difficult to achieve in a strictly reproducible manner. A luminescence study is expected to be a promising tool for checking non-destructively the quality of the sheets, because efficient low-temperature luminescence of AgCl, sensitive to various lattice defects and impurities, has been known for a long time. We have already published a study dealing with the use of luminescence spectroscopy to monitor the aging of AgCl:Cd^{2+} sheets [4].

† Present address: Institute of Physics, Czech Academy of Sciences, Cukrovarnická 10, 162 00 Prague 6, Czech Republic.

‡ Joint Institute for Nuclear Research, Dubna, Russia.

0953-8984/95/020433+14$19.50

In this paper are described the results of our measurements of time-resolved photoluminescence spectra at various temperatures from ~ 20 to 80 K. All experiments were carried out on solid-state crystalline foils of both pure AgCl sheets and AgCl doped with cadmium (Cd^{2+}). It turns out that crystalline AgCl:Cd^{2+} sheets have quite unique photoluminescence properties, in particular for time-resolved photoluminescence (long decay time, enormous red shift with delay). Our goal is to submit a microscopic model explaining the main features of the observed time-resolved luminescence behaviour and to suggest a simple luminescence test for how to predict the suitability of a given AgCl:Cd^{2+} sheet to record high-energy-particle tracks.

The paper is organized as follows. Section 2 deals with experimental details and main experimental results. Section 3 contains a microscopic model of emission centres in the framework of a configuration coordinate, supported by simple kinetic equations. Discussion of the results and link with detector suitability are subjects of section 4.

2. Experiment

2.1. Experimental set-up

Silver chloride crystalline sheets were grown by a sandwich method, i.e. by melting the AgCl precipitate (prepared from silver nitrate and hydrochloric acid solution using special pure chemical reagents) and allowing the melt to leak into a space between two glass plates by the action of capillary forces. Dopant ions were added to the molten phase in the form of $CdCl_2$. Nominal concentrations of Cd^{2+} cations ranged from 62.5 to 5000 ppm. The sheets, prepared in air, were subsequently rolled out between Cr-coated metallic rollers into the form of thin foils of typical thickness 0.1–0.5 mm (this is a procedure indispensable to increase the sensitivity of AgCl:Cd^{2+} detectors and/or the quality of particle tracks [5]). Finally, samples with dimensions of $\sim 5 \times 8$ mm^2 used for luminescence studies were cut from the foils.

Luminescence was excited by a 200 W high-pressure mercury lamp supplied with a UG1 filter (band→band excitation). Luminescence radiation was dispersed by an $f/4.2$ grating monochromator (dispersion 4 nm mm^{-1}) and detected with a quantacon-type photomultiplier (Hamamatsu R928). The output signal from the photomultiplier was fed into a lock-in amplifier. Emission spectra were corrected for the spectral response of the apparatus. Most of the time-resolved photoluminescence experiments were carried out using a mechanical phosphoroscope with two mechanical choppers, one of them being located in excitation and the other in emission paths. The phase shift between the chopper discs was controlled by a synchronization unit. A gate with time width adjustable between 14 and 210 ms sampled the photoluminescence signal with variable delay of 3–220 ms (i.e. time interval between the end of excitation window and the opening of the gate). Alternatively, a time-correlated photon-counting technique in conjunction with a pulsed halogen-lamp excitation were used to measure directly the luminescence decay curves. The AgCl samples were mounted in an exchange He gas of a temperature-variable gas-flow cryostat. Temperature was measured by an Allen-Bradley resistor.

2.2. Experimental results

An overall view of photoluminescence spectra of AgCl:Cd^{2+} foils with various Cd^{2+} concentration, taken at 75 K, is shown in figure 1. The spectra have been recorded synchronously with the excitation pulse. The spectrum has a form of a single wide

structureless band, with maximum located at ~ 480 nm in nominally pure AgCl, shifting gradually to the red region as the Cd^{2+} concentration increases. However, this shift reaches its maximum at Cd^{2+} concentration 250–1000 ppm and then the band maximum returns gradually to the blue region.

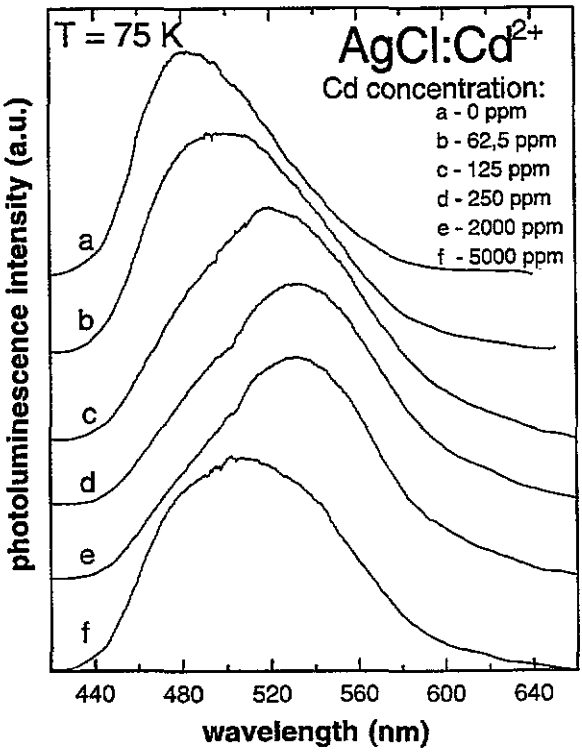

Figure 1. Photoluminescence spectra of AgCl:Cd^{2+} foils with different Cd^{2+} concentrations. Spectra were detected in time coincidence with excitation at $T = 75$ K. The large red shift reaches its maximum for dopant concentrations of about 500 ppm.

Figure 2 shows time-resolved photoluminescence spectra of AgCl:Cd^{2+} with Cd^{2+} concentration of 500 ppm, taken also at constant temperature of $T = 75$ K. The spectra are normalized in such a manner that the area below the curves remains constant. Note that the spectra intersect at one point with high precision; we shall discuss this point later on. It is clearly seen from figure 2 that the emission sweeps markedly to the red with increasing gate delay: a second band ('red') located at ~ 600 nm appears and grows gradually whereas the 'blue' band decays comparatively rapidly. This change of emission wavelength can be observed also by the naked eye; a simple photoluminescence decay experiment (mechanical excitation radiation cut-off) results in gradual change of the luminescence colour from blue-green to dark red within ~ 1 s, which is a rather striking effect.

Keeping the gate delay constant but now varying the temperature leads to a set of emission spectra shown in figure 3(*a*). Like in figure 2, the emission spectrum becomes red-shifted as the temperature increases. Particularly sensitive turned out to be the temperature range ~ 45–65 K, where substantial modifications of the spectrum occur. It is evident that one can again separate two components of the spectrum, a 'blue' and a 'red' one,

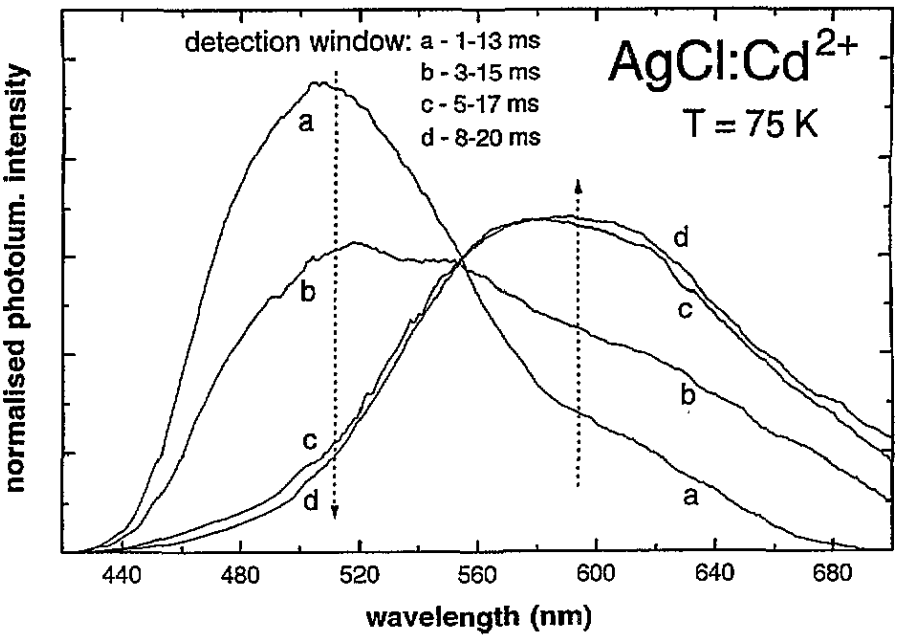

Figure 2. Time-resolved photoluminescence spectra of AgCl:Cd^{2+} foils (500 ppm Cd^{2+}) at $T = 75$ K. Each spectrum is normalized to equal integral intensity. The blue component of emission decreases to the benefit of the red component with increasing delay (arrows). The intersection of normalized spectra at one point proves that just two luminescence species are involved in emission.

and to plot integrated intensities of each of them versus temperature. This is done in figure 3(*b*) (crosses and triangles). Our point of view—namely that we deal with only two radiative centres—is justified by figure 2: intersection of time-resolved emission spectra at one point means that *just two emission species are involved in luminescence radiation* [6] (see appendix 1). Decomposition of the spectra from figure 3(*a*) could involve, of course, considerable arbitrariness. To minimize it, we proceed as follows: we suppose the delayed spectra of AgCl:Cd^{2+} measured at sufficiently high temperature (spectrum f in figure 3(*a*)) to be a 'pure' spectrum of the red component, because its shape does not depend on delay and temperature (if they are sufficiently high). This shape can be mathematically expressed as a sum of three Gaussian bands centred at 566, 608 and 672 nm with fixed intensity ratio. At low temperatures and for shorter delays, the blue emission comes to dominate the spectra. After subtracting the red component, the blue band can be described as a sum of another two Gaussians centred at 498 and 532 nm. We take the sum of the first three Gaussian areas as the experimental value of the integrated intensity I_R of the red component and the areas of the two additional Gaussians give the experimental integrated intensity of the blue component, which we denote I'_B. The Gaussians mentioned above *serve only as a helping mathematical tool for the decomposition procedure*, without true physical meaning.

The dependences depicted in figure 3(*b*) present the main result of this work and simultaneously a challenge of how to explain them. In section 3 we put forward a simple microscopic model of energy transfer between two radiative centres. Before we proceed to this end, we present in figure 4 decay curves of the blue and red components, measured at $T = 75$ K. The decay is to a good approximation single-exponential in the case of both blue

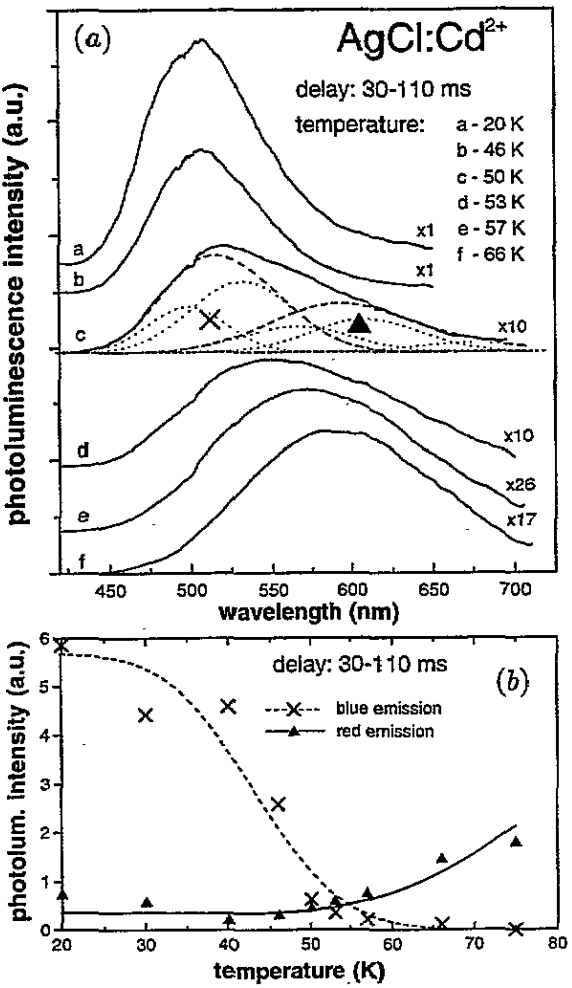

Figure 3. Temperature changes of photoluminescence of AgCl:Cd^{2+} foils (500 ppm Cd^{2+}) detected within 30–110 ms time window after excitation. (*a*) Photoluminescence spectra taken at six different temperatures. The decomposition into the blue band (sum of two Gaussians) and red band (sum of three Gaussians) is shown for spectrum c (broken and dotted bands). (*b*) Integrated photoluminescence intensities versus temperature of blue component (crosses) and of red component (triangles). The best theoretical fits obtained using equations (6*a*) and (6*b*) are indicated by a broken curve (blue component) and by a full curve (red component). The corresponding fitting parameters are: $\nu = 1.3 \times 10^2\ s^{-1}$, $E_A = 45$ meV, $\mu = 3.7 \times 10^3\ s^{-1}$, $E_Q = 22$ meV, $\tau_r^B = 13$ ms and $g = 0.001$.

and red components. One can thus find corresponding luminescence lifetimes τ_0^B and τ_0^R describing satisfactorily the observed decay curves as $\sim \exp(-t/\tau_0^{B(R)})$, where $\tau_0^B = 5.8$ ms and $\tau_0^B = 100$ ms are related to the blue and red components, respectively.

3. Model of luminescence centres: energy transfer

Low-temperature photoluminescence of pure AgCl crystals has been known for a long time

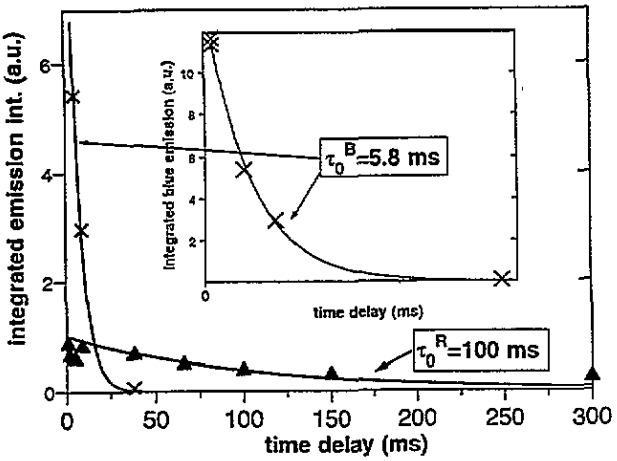

Figure 4. Photoluminescence decay curves of integrated intensities of the blue (crosses) and the red (triangles) components taken at $T = 75$ K. The exponential fits $I(t) = \text{const} \times \exp(-t/\tau)$ are shown by full curves. The inset shows the decay of the blue component in detail.

[7, 8]. It is characterized by a wide blue-green band at ~ 480 nm. Radiative decay of a self-trapped exciton (STE) (self-trapped hole $(AgCl_6)^{4-}$ plus electron) is generally accepted to be responsible for this light emission [8]. The appearance of a very similar band in the time-resolved spectra of our Cd-doped samples indicates that this luminescence centre remains basically intact and functional also in AgCl:Cd^{2+}. Divalent impurities in AgCl are known to cause red-shifted luminescence bands [9]. It is therefore obvious to suppose that the red band found in our experiments (figures 2 and 3(*a*)) is due to a Cd^{2+} ion-related emission. Moreover, the gradual continuous shift of luminescence from the blue to the red as a function of both time delay and temperature suggests the idea of thermally activated energy transfer. A corresponding possible microscopic scheme is schematically depicted in figure 5. Taking into consideration the high Cd^{2+} concentration in our samples, the occurrence of geminate pairs STE/Cd^{2+} like in figure 5(*a*) is quite probable. The relevant configuration coordinate diagram is shown in figure 5(*b*). Band→band photoexcitation is followed by fast relaxation to the STE band [10] and then thermally activated transfer over the barrier E_A or thermal quenching of the blue STE emission with an activation energy E_Q can occur. As a result, two wide emission bands, 'blue' and 'red', are found.

The processes described above are governed by the following kinetic equations. Let n_B and n_R be concentrations of the blue and red luminescence centres, respectively. Then we can write

$$\begin{aligned} \mathrm{d}n_B/\mathrm{d}t &= G + (\mathrm{d}n_B/\mathrm{d}t)_r + (\mathrm{d}n_B/\mathrm{d}t)_{nr} - \nu n_B \exp(-E_A/kT) \\ \mathrm{d}n_R/\mathrm{d}t &= \nu n_B \exp(-E_A/kT) + (\mathrm{d}n_R/\mathrm{d}t)_r + (\mathrm{d}n_R/\mathrm{d}t)_{nr}. \end{aligned} \tag{1}$$

Here G means generation rate of electron–hole pairs, $(\mathrm{d}n/\mathrm{d}t)_r$ and $(\mathrm{d}n/\mathrm{d}t)_{nr}$ are radiative and non-radiative recombination rates, and $\nu \exp(-E_A/kT)$ is the probability density of overcoming the potential barrier for E_A. For radiative and non-radiative recombination rates in (1) we write

$$(\mathrm{d}n_B/\mathrm{d}t)_r + (\mathrm{d}n_B/\mathrm{d}t)_{nr} = -[1/\tau_r^B + \mu \exp(-E_Q/kT)]n_B$$

$$(\mathrm{d}n_R/\mathrm{d}t)_r + (\mathrm{d}n_R/\mathrm{d}t)_{nr} = -n_R/\tau_r^R$$

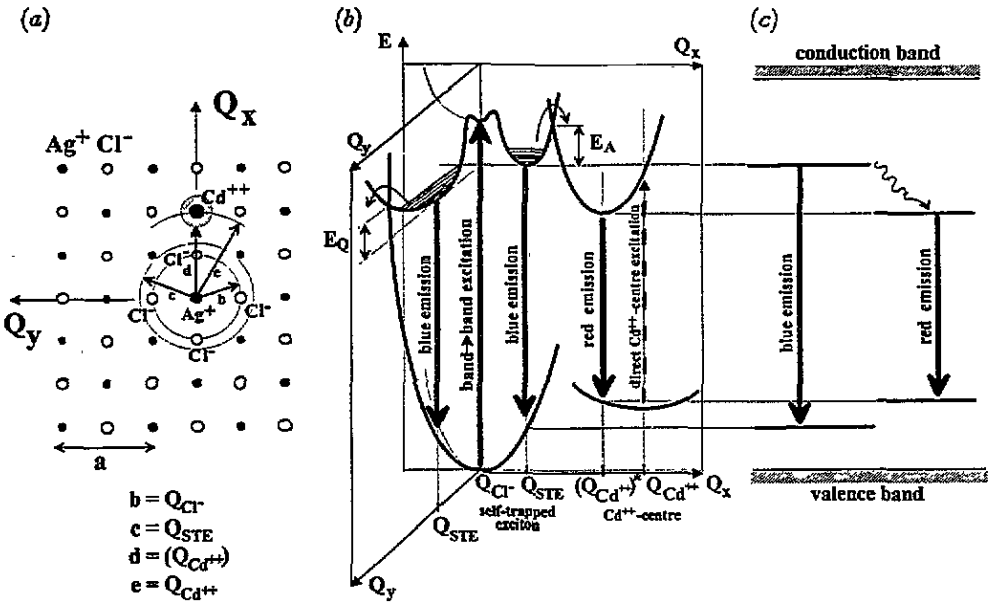

Figure 5. Microscopic model of energy transfer between STE and Cd^{2+} centre. (*a*) Microscopic scheme of STE centre with Cd^{2+} ion in the nearest-neighbour position. (*b*) Configuration coordinate diagram. Two possible paths of STE de-excitation: the non-radiative transfer of excitation energy to the Cd^{2+} centre and non-radiative decay are shown in Q_x plane and Q_y plane, respectively. (*c*) Simplified energy level scheme.

where we neglect non-radiative recombination in the red luminescence centre, an approximation justifiable in the investigated temperature range. Here τ_r^B and τ_r^R mean radiative lifetimes. Then equations (1) take the form

$$\begin{aligned} dn_B/dt &= G - n_B[1/\tau_r^B + \mu \exp(-E_Q/kT) + \nu \exp(-E_A/kT)] \\ dn_R/dt &= -n_R/\tau_r^R + n_B \nu \exp(-E_A/kT). \end{aligned} \tag{1a}$$

A solution of (1*a*) for the case of photoluminescence decay, i.e. when $G = 0$ at $t = 0$, is

$$\begin{aligned} n_B(t,T) &= n_B(0,T) \exp\left[-t\left(\frac{1}{\tau_r^B} + Q + A\right)\right] \\ &= n_B(0,T) \exp\left(-\frac{t}{\tau_0^B}\right) \\ n_R(t,T) &= \left(n_R(0,T) + \frac{An_B(0,T)}{1/\tau_0^B - 1/\tau_r^R}\right) \exp\left(-\frac{t}{\tau_r^R}\right) - \frac{An_B(0,T)}{1/\tau_0^B - 1/\tau_r^R} \exp\left(-\frac{t}{\tau_0^B}\right) \end{aligned}$$

where $A = \nu \exp(-E_A/kT)$ and $Q = \mu \exp(-E_Q/kT)$. Taking $I_{B(R)} = n_{B(R)}/\tau_r^{B(R)}$ for corresponding luminescence intensities, we have

$$I_B(t,T) = \frac{n_B(t,T)}{\tau_r^B}$$
$$= \frac{n_B(0,T)}{\tau_r^B}\exp\left[-t\left(\frac{1}{\tau_r^B} + A + Q\right)\right] \tag{2a}$$
$$= \frac{n_B(0,T)}{\tau_r^B}\exp\left(-\frac{t}{\tau_0^B}\right)$$

$$I_R(t,T) = \frac{n_R(t,T)}{\tau_r^R}$$
$$= \frac{1}{\tau_r^R}\left(n_R(0,T) + \frac{An_B(0,T)}{1/\tau_0^B - 1/\tau_r^R}\right)\exp\left(-\frac{t}{\tau_r^R}\right) \tag{2b}$$
$$- \frac{An_B(0,T)}{\tau_r^R(1/\tau_0^B - 1/\tau_r^R)}\exp\left(-\frac{t}{\tau_0^B}\right).$$

Let us note that the blue emission intensity I_B defined in this way does not yet mean the experimentally measured value that we denote I'_B (see below).

Now we wish to find solution of (1*a*) for the stationary regime, i.e. $G \neq 0$, $n_R(t,T) = n_R(0,T)$, $n_B(t,T) = n_B(0,T)$ and $dn_B/dt = dn_R/dt = 0$. First, from (1*a*) we obtain immediately

$$n_B(0,T) = G/(1/\tau_r^B + A + Q) \tag{3a}$$

and

$$n_R(0,T) = \tau_r^R n_B(0,T)A. \tag{3b}$$

Finally, substituting (3*a*) into (2*a*) gives

$$I_B(t,T) = \frac{G}{\tau_r^B(1/\tau_r^B + A + Q)}\exp\left[-t\left(\frac{1}{\tau_r^B} + A + Q\right)\right] = \frac{G}{\tau_r^B/\tau_0^B}\exp\left(-\frac{t}{\tau_0^B}\right) \tag{4a}$$

and substituting (3*a*) and (3*b*) into (2*b*) yields

$$I_R(t,T) = \frac{GA}{\tau_r^R(1/\tau_r^B + A + Q)}\left[\left(\tau_r^R + \frac{1}{1/\tau_0^B - 1/\tau_r^R}\right)\exp\left(-\frac{t}{\tau_r^R}\right)\right.$$
$$\left. - \frac{1}{1/\tau_0^B - 1/\tau_r^R}\exp\left(-\frac{t}{\tau_0^B}\right)\right]. \tag{4b}$$

Equations (4) should correctly describe our experimental results both on luminescence kinetics (figure 4) and temperature dependence (figure 3). However, it follows from (4*b*) for sufficiently low temperature, when $A \to 0$ and $Q \to 0$, that $I_R(t,0) \to 0$. The red photoluminescence thus should not be present at helium temperatures at all. This is not the case, though. Our experimental results at $T = 10$ K imply that there is still (even if very weak) a red component—see figure 3(*b*). It suggests the existence of another energy transfer channel, independent of temperature. The most probable one is resonant reabsorption of the blue emission in red-related Cd^{2+} centres (broken vertical line in figure 5(*b*)). To verify this conjecture, we performed experiments dealing with photoluminescence excitation with

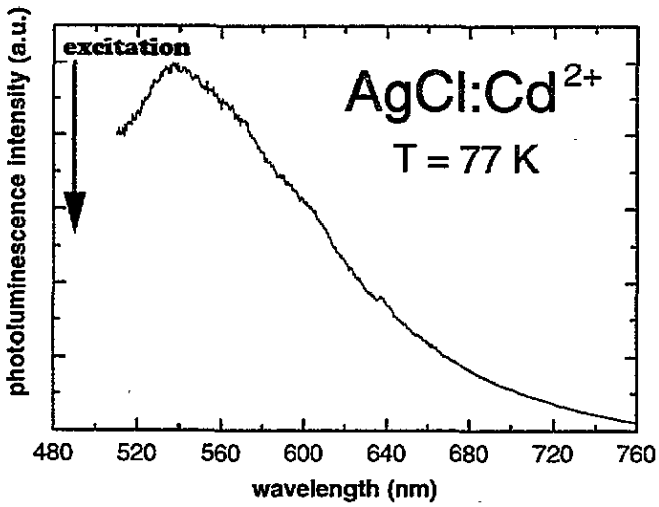

Figure 6. Photoluminescence spectrum of AgCl:Cd^{2+} foil (500 ppm Cd^{2+}) excited by Ar^+-laser line at 488 nm, i.e. far below direct AgCl band→band transition. No time delays were introduced between excitation and detection.

a blue Ar^+-laser line $\sim$ 488 nm. A wide emission band extending to the red region has really appeared (figure 6), proving the existence of resonant reabsorption energy transfer.

The simplest way to implement the resonant reabsorption into our equations is simply to add a term $\alpha(t,T)I_B(t,T)$, where $\alpha(t,T)$ is a phenomenological coefficient describing the reabsorption effects, into (4*b*). We obtain

$$I_R(t,T) = \frac{GA}{\tau_r^R(1/\tau_r^R + A + Q)}\left[\left(\tau_r^R + \frac{1}{1/\tau_0^B - 1/\tau_r^R}\right)\exp\left(-\frac{t}{\tau_r^R}\right) - \frac{1}{1/\tau_0^B - 1/\tau_r^R}\exp\left(-\frac{t}{\tau_0^B}\right)\right] + \alpha(t,T)I_B(t,T). \tag{5}$$

We can find an explicit form of $\alpha(t,T)$ if we incorporate a new microscopic generation term $dn_R/dt = gI_B(t,T)$ directly into the kinetic equation (1*a*). This exact treatment is described in appendix 2. Moreover, we must now also consider lowering of the blue emission $I_B(t,T)$ caused by the absorption in the impurity centres (resonant reabsorption) (see appendix 2). The final equations will be

$$I'_B(t,T) = \frac{G}{\tau_r^B/\tau_0^B}\left[1 + g\left(\frac{2}{\tau_r^R/\tau_0^B - 1} - \frac{\tau_r^R}{\tau_0^B}\right)\right]\exp\left(-\frac{t}{\tau_0^B}\right) \tag{6a}$$

$$I_R(t,T) = \frac{G}{\tau_r^R(1/\tau_r^B + A + Q)}\left[\left(\tau_r^R + \frac{1}{1/\tau_0^B - 1/\tau_r^R}\right)\exp\left(-\frac{t}{\tau_r^R}\right) - \frac{1}{1/\tau_0^B - 1/\tau_r^R}\exp\left(-\frac{t}{\tau_0^B}\right)\right]\left(A + \frac{g}{\tau_r^B}\right) \tag{6b}$$

where $I'_B(t,T)$ denotes the experimentally detectable blue intensity.

4. Discussion

We wish to demonstrate now that the equations (6*a*) and (6*b*) explain well our experimental results.

4.1. Time-resolved photoluminescence spectra at constant T

The blue component decay should be governed, according to (6*a*), by an exponential law. This is what can be seen from figure 4(*a*). The red component (6*b*) contains two exponential terms. Because we introduce in our model (1*a*) no quenching of the red band, it follows that $\tau_r^R = \tau_0^R$. Taking then into consideration the values of $\tau_0^B = 5.8$ ms and $\tau_0^R = 100$ ms, we find that $\tau_r^R \gg (1/\tau_0^B - 1/\tau_r^R)^{-1}$ and we can thus neglect the second term in the square brackets in (6*b*). At sufficiently long times, the decay curve is governed by the first term in (6*b*), i.e. by the exponential law $\sim \exp(-t/\tau_0^R)$, thus showing the self-consistency of our analysis.

4.2. Intensities of both emission bands as a function of T at t = constant

To compare the experimental results (points) in figure 3(*b*) with equation (6), we put into (6*a*) and (6*b*) the values $t = 70$ ms, $T = 75$ K, $\tau_r^R = \tau_0^R = 100$ ms and $\tau_0^B = 5.8$ ms. Six unknown parameters then remain in (6): ν, E_A, μ, E_B, τ_r^B and g. They are, nevertheless, constrained by the condition $1/\tau_0^B = 1/\tau_r^B + \nu \exp(-E_A/kT) + \mu \exp(-E_Q/kT)$. Allowing these parameter to vary, we obtain the theoretical curves $I'_B(T)$ and $I_R(T)$ shown in figure 3(*b*) by broken and full curves, respectively. The agreement with the experimental points is reasonably good, in view of the simplicity of our model and of the arbitrariness involved in the decomposition of the overall emission spectrum into two components. The best fit in figure (3(*b*)) yields the following set of parameters: $\nu = 1.3 \times 10^2$ s^{-1}, $E_A = 45$ meV, $\mu = 3.7 \times 10^3$ s^{-1}, $E_Q = 22$ meV, $\tau_r^B = 13$ ms and $g = 0.001$. It should be stressed that, besides the arbitrary value of G, no additional scaling factors have been used in plotting the curves in figure 3(*b*).

The extremely low values of the pre-exponential factors ν and μ are worth mentioning. Similar low values of ν have been found recently in porous silicon [11], which also exhibits unusual long luminescence decay times ($\sim 10^{-3}$ s at $T = 10$ K). This indicates that both radiative and non-radiative processes have low efficiencies. In comparison with the luminescence of pure AgCl crystals [12], the decay rates are slowed down by at least two orders of magnitude. The reason for such behaviour remains unclear at present. Nevertheless, one possible explanation can be put forward, namely the passivation of dislocations, which act as non-radiative centres in AgCl, by the formation of a positive point-charge (Cd^{2+}) atmosphere around the dislocations [13]. This can lead to a substantial decrease of non-radiative decay rate.

The shift of the maximum of the prompt photoluminescence spectra with changing Cd^{2+} concentration (figure 1) can be explained as a consequence of the different concentration of 'red' luminescence centres containing a Cd^{2+} ion incorporated into cationic lattice substitutional sites. This concentration determines the intensity of the red emission. For Cd^{2+} concentrations below ~ 250 ppm the potential number of Cd^{2+} luminescence centres is not saturated [5], whereas for concentrations higher than 1000 ppm a precipitation of Cd ions, and consequently, concentration quenching of the red band is probable, which results in backward blue shift.

A final remark concerns the possibility of using time-resolved spectroscopy to check the suitability of AgCl:Cd^{2+} foils to record high-energy-particle tracks. A frequently

encountered drawback of these detectors is track inhomogeneity, following predominantly from concentration inhomogeneity (precipitation) of Cd^{2+} ions. It is known experimentally, on the other hand, that the foils with concentration range 500–1000 ppm of Cd^{2+} exhibit the highest sensitivity, provided the Cd^{2+} ions are homogeneously dispersed. Figure 7 shows the ratio of intensities of delayed emission at $\lambda = 540$ nm to prompt emission at $\lambda = 510$ nm as a function of Cd^{2+} concentration. It can be seen that this function exhibits a distinct maximum just at 500–1000 ppm Cd^{2+}. We can therefore apply time-resolved photoluminescence spectroscopy, if necessary combined with high spatial resolution (excitation by e.g. He–Cd laser), to verify whether the true Cd^{2+} concentration corresponds to the nominal one, to check its homogeneity and to rule out unsuitable foils prior to their use in recording particle tracks.

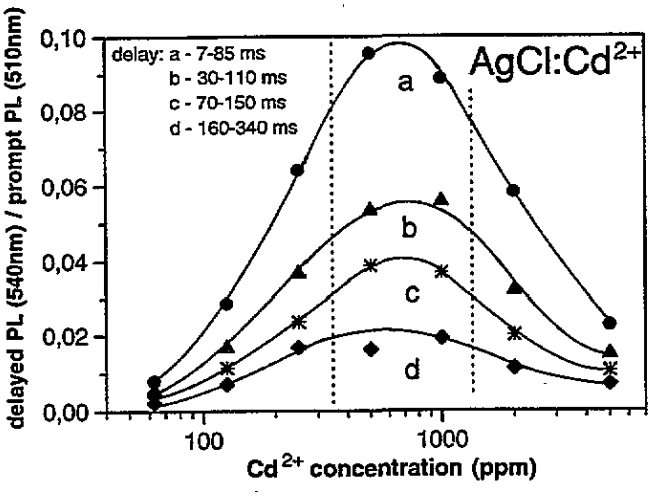

Figure 7. Ratio of intensities of delayed emission at $\lambda = 540$ nm to prompt emission at $\lambda = 510$ nm versus Cd^{2+} concentration. The slowly decayed red component of the emission spectrum reaches the highest intensity for Cd^{2+} concentrations of 500 and 1000 ppm.

5. Conclusion

In conclusion, we have applied low-temperature time-resolved photoluminescence spectroscopy to study radiative and non-radiative recombination channels in AgCl:Cd^{2+} foils. Our results brought out evidence of two types of luminescence centres, intrinsic (STE) and extrinsic (Cd^{2+} related) ones. Two mechanisms of energy transfer between the centres, thermally activated and resonant temperature-independent ones, have been found. A method of photoluminescence diagnostics of AgCl:Cd^{2+} solid-state nuclear-track detectors has been suggested.

Appendix 1. Spectral response of multi-component mixture

Let n different emission centres contribute to emission of some material. Each component is characterized by emission curve $g_i(x)$ (x denotes any spectral variable, e.g. wavelength,

energy of wavenumber). Suppose integrals of these functions on the interval of measurement $\langle x_L, x_H \rangle$ are normalized to unity, i.e.

$$\int_{x_L}^{x_H} g_i(x)\,dx = 1 \qquad i = 1, \ldots, n. \tag{A1.1}$$

Performing time-resolved spectral measurement at different delays after excitation, we obtain a series of spectra $h_q(x)$ and we normalize them also to unity on $\langle x_L, x_H \rangle$. Experimental spectrum $h_q(x)$ is a sum of n basic emission components g_i

$$h_q(x) = \alpha_1 g_1(x) + \cdots + \alpha_n g_n(x) = \sum_{i=1}^{n} \alpha_i g_i(x).$$

Here α (time-dependent in the case of time-resolved emission spectra) represents the concentration vector of the emission centres in the spectral mixture. As both function $g_i(x)$ and $h_q(x)$ are normalized to unity on $\langle x_L, x_H \rangle$, by integration of A1.1 it follows that

$$\sum_{i=1}^{n} \alpha_i = 1.$$

Let us suppose that all (normalized) experimental spectra $h_q(x)$ intersect at one point, i.e. they have an equal value $h_q(x_E)$ at the point x_E. This condition is equivalent to the invariance of the function $h_q(x) = \sum \alpha_i g_i(x)$ with respect to the vector α at the point x_E. In that case, we can take $\alpha = (1, 0, \ldots, 0)$, $\alpha = (0, 1, 0, \ldots, 0), \ldots$, and the existence of an intersection in experimental spectra is equivalent to the condition

$$h_q(x_E) = \sum_{i=1}^{n} \alpha_i g_i(x_E) = g_j(x_E) \qquad j = 1, \ldots, n.$$

For one- ($n = 1$) and two-component ($n = 2$) spectral mixtures, this condition is satisfied automatically. In case of three or more spectral components, they cannot generally intersect at one point if they have approximately equal shape and width.

In conclusion, if all (at least three) normalized experimental time-resolved spectra $h_q(x)$ of an unknown spectral mixture cross each other at one point at least, one has to deal with a two-component mixture.

Appendix 2. Incorporation of resonant reabsorption into the kinetic equations

We add a new generation rate $gI_B = gn_B/\tau_r^B$ into equation (1*a*) for dn_R/dt:

$$dn_R/dt = -n_R/\tau_r^R + n_B[\nu \exp(-E_A/kT) + g/\tau_r^B]. \tag{A2.1}$$

A solution of (A2.1) for the case of photoluminescence decay ($G = 0$ at $t = 0$) is

$$n_R(t, T) = \left(n_R(0, T) + \frac{n_B(0, T)(A + g/\tau_r^B)}{1/\tau_0^B - 1/\tau_r^R}\right) \exp\left(-\frac{t}{\tau_r^R}\right) - \frac{n_B(0, T)(A + g/\tau_r^B)}{1/\tau_0^B - 1/\tau_r^R} \exp\left(-\frac{t}{\tau_0^B}\right) \tag{A2.2}$$

where $A = \nu \exp(-E_A/kT)$. Taking $I_R = n_R(t, T)/\tau_r^R$ for red luminescence intensity, we have

$$I_R(t,T) = \frac{1}{\tau_r^R}\left(n_R(0,T) + \frac{n_B(0,T)(A + g/\tau_r^B)}{1/\tau_0^B - 1/\tau_r^R}\right)\exp\left(-\frac{t}{\tau_r^R}\right) - \frac{n_B(0,T)(A+g/\tau_r^B)}{\tau_r^R(1/\tau_0^B - 1/\tau_r^R)}\exp\left(-\frac{t}{\tau_0^B}\right). \tag{A2.3}$$

For the stationary regime ($G \neq 0$, $n_R(t,T) = n_R(0,T)$ and $dn_R/dt = 0$) we obtain from (A2.1)

$$n_R(0,T) = \tau_r^R n_B(0,T)(A + g/\tau_r^B). \tag{A2.4}$$

Substituting (3*a*) and (A2.4) into (A2.3) gives

$$I_R(t,T) = \frac{GA}{\tau_r^R(1/\tau_r^B + A + Q)}\left[\left(\tau_r^R + \frac{1}{1/\tau_0^B - 1/\tau_r^R}\right)\exp\left(-\frac{t}{\tau_r^R}\right) - \frac{1}{1/\tau_0^B - 1/\tau_r^R}\exp\left(-\frac{t}{\tau_0^B}\right)\right] + \frac{gG}{\tau_r^B}\frac{1}{\tau_r^R(1/\tau_r^B + A + Q)} \times \left[\left(\tau_r^R + \frac{1}{1/\tau_0^B - 1/\tau_r^R}\right)\exp\left(-\frac{t}{\tau_r^R}\right) - \frac{1}{1/\tau_0^B - 1/\tau_r^R}\exp\left(-\frac{t}{\tau_0^B}\right)\right] \tag{A2.5}$$

where the first term is the same as in (4*b*) and the second term can be written in the form $\alpha(t,T)I_B(t,T)$ using (4*a*). We obtain an expression that is formally identical with equation (5) where

$$\alpha(t,T) = \frac{g}{\tau_r^R}\left\{\left(\tau_r^R + \frac{1}{1/\tau_0^B - 1/\tau_r^R}\right)\exp\left[+t\left(\frac{1}{\tau_0^B} - \frac{1}{\tau_r^R}\right)\right] - \frac{1}{1/\tau_0^B - 1/\tau_r^R}\right\}. \tag{A2.6}$$

More rigorous mathematical treatment leads therefore to the same result like the phenomenological approach applied in section 3.

Now, we should consider that the intensity of blue emission $I'_B(t,T)$ is reduced with respect to $I_B(t,T)$ due to the resonant reabsorption. In the simplest approximation, we suppose $I'_B(t,T) = \eta I_B(t,T)$, where $0 < \eta < 1$. The explicit form of η as a function of g we can deduce from the following integral equation:

$$\int_0^\infty I_B(t,T)\,dt = \int_0^\infty \eta I_B(t,T)\,dt + \int_0^\infty \alpha(t,T)I_B(t,T)\,dt. \tag{A2.7}$$

In this equation, the left-hand side represents the total number of blue photons emitted after the end of excitation and the right-hand side terms represent the number of blue photons leaving the sample and the number of blue photons absorbed in red centres, respectively. Substituting (4*a*) and (A2.6) into (A2.7) yields

$$\eta(T) = 1 - g\left(\frac{\tau_r^R}{\tau_0^B} - \frac{2}{\tau_r^R/\tau_r^B - 1}\right). \tag{A2.8}$$

Note that without reabsorption ($g = 0$) $\eta(T) = 1$ and $I'_B(t,T) = I_B(t,T)$, as expected. Finally, the equation for measurable blue emission intensity will be

$$I'_B(t,T) = \frac{G}{\tau_r^B/\tau_0^B}\left[1 + g\left(\frac{2}{\tau_r^R/\tau_0^B - 1} - \frac{\tau_r^R}{\tau_0^B}\right)\right]\exp\left(-\frac{t}{\tau_0^B}\right). \tag{A2.9}$$

The expressions (A2.5) and (A2.9) correspond to the expressions (6*b*) and (6*a*), respectively. They are used in figure 3 to calculate the theoretical temperature dependences of the red and blue emission bands.

References

[1] Haase G, Schopper E and Granzer F 1977 *Radiat. Effects* **34** 25

[2] Baican B, Schopper E and Schott J U 1986 *Int. J. Radiat. Appl. Instrum.* D **12** 519
Kranz A R, Gartenbach K, Zimmermann M, Schopper E, Baican B, Wendnagel Th, Schott J U and Heilmann C 1992 *Int. J. Radiat. Appl. Instrum.* D **20** 217

[3] Bradna F, Bradnová V, Jukl F and Dobržanskij G F 1984 *Communication of the Joint Institute for Nuclear Research* 12-84-276, Dubna (in Russian)

[4] Valenta J, Bradnová V, Kohlová V, Jukl F, Kulikova S I, Nevzorova N M and Pelant I 1990 *Radiat. Effects Defects Solids* **114** 333

[5] Granzer F, Schopper E and Wendnagel Th 1980 *Proc. 10th Int. Conf. on Solid State Nuclear Track Detectors (Lyon, 1979)* ed H Francois *et al* (Oxford: Pergamon) p 57

[6] Klimovič J 1984 *Proc. Summer School—Modern Spectroscopic Methods in Chemical Physics and Biophysics (Luhačovice)* p 58

[7] Vacek K 1960 *Proc. Int. Conf. on Semiconductor Physics (Prague)* p 682

[8] Williams R T and Song K S 1990 *J. Phys. Chem. Solids* **51** 679

[9] Sonioke S and Akimoto K 1961 *J. Phys. Soc. Japan* **16** 658

[10] Laredo E, Rowan L G and Slifkin L 1981 *Phys. Rev. Lett.* 47 384
Pelant I and Hála J 1991 *Solid State Commun.* **78** 141

[11] Amato G 1994 *Solid State Commun.* **89** 213

[12] Burberry M S and Marchetti A P 1985 *Phys. Rev.* B **32** 1192

[13] Wendnagel Th, Schopper E and Granzer F 1980 *Proc. 10th Int. Conf. on Solid State Nuclear Track Detectors (Lyon, 1979)* ed H Francois *et al* (Oxford: Pergamon) p 147